HAL
archives-ouvertes.fr

Short Note The Burst-Like Behavior of Aseismic Slip on a Rough Fault: The Creeping Section of the Haiyuan Fault, China

R Jolivet, T Candela, C Lasserre, F Renard, Y Klinger, M.-P Doin

▶ To cite this version:

R Jolivet, T Candela, C Lasserre, F Renard, Y Klinger, et al.. Short Note The Burst-Like Behavior of Aseismic Slip on a Rough Fault: The Creeping Section of the Haiyuan Fault, China. Bulletin of the Seismological Society of America, Seismological Society of America, 2014, 105 (1), pp.480-488. 10.1785/0120140237 . insu-01302143

HAL Id: insu-01302143

https://hal-insu.archives-ouvertes.fr/insu-01302143

Submitted on 13 Apr 2016

HAL is a multi-disciplinary open access archive for the deposit and dissemination of scientific research documents, whether they are published or not. The documents may come from teaching and research institutions in France or abroad, or from public or private research centers.

L'archive ouverte pluridisciplinaire **HAL**, est destinée au dépôt et à la diffusion de documents scientifiques de niveau recherche, publiés ou non, émanant des établissements d'enseignement et de recherche français ou étrangers, des laboratoires publics ou privés.

Bulletin of the Seismological Society of America, Vol. 105, No. 1, pp. 480–488, February 2015, doi: 10.1785/0120140237

Short Note

The Burst-Like Behavior of Aseismic Slip on a Rough Fault: The Creeping Section of the Haiyuan Fault, China

by R. Jolivet,* T. Candela, C. Lasserre, F. Renard,† Y. Klinger, and M.-P. Doin

Abstract Recent observations suggesting the influence of creep on earthquakes nucleation and arrest are strong incentives to investigate the physical mechanisms controlling how active faults slip. We focus here on deriving generic characteristics of shallow creep along the Haiyuan fault, a major strike-slip fault in China, by investigating the relationship between fault slip and geometry. We use optical images and time series of Synthetic Aperture Radar data to map the surface fault trace and the spatiotemporal distribution of surface slip along the creeping section of the Haiyuan fault. The fault trace roughness shows a power-law behavior similar to that of the aseismic slip distribution, with a 0.8 roughness exponent, typical of a self-affine regime. One possible interpretation is that fault geometry controls to some extent the distribution of aseismic slip, as it has been shown previously for coseismic slip along active faults. Creep is characterized by local fluctuations in rates that we define as creep bursts. The potency of creep bursts follows a power-law behavior similar to the Gutenberg–Richter earthquake distribution, whereas the distribution of bursts velocity is non-Gaussian, suggesting an avalanche-like behavior of these slip events. Such similarities with earthquakes and lab experiments lead us to interpret the rich dynamics of creep bursts observed along the Haiyuan fault as resulting from long-range elastic interactions within the heterogeneous Earth's crust.

Introduction

Understanding what controls the initiation, the propagation, and the arrest of an earthquake has become one of the key issues in earthquake mechanics (King and Nabelek, 1985; Wesnousky, 2006; Klinger, 2010). Effective models can reproduce the apparent segmentation of faults during all phases of the earthquake cycle (Barbot *et al.*, 2012). However, in terms of physical mechanisms, friction does not seem to be the only process involved, as the exploration of coseismic slip lateral variations along faults (Lasserre *et al.*, 2005) as well as mechanical studies of rupture processes (Adda-Bedia and Madariaga, 2008) have also highlighted the role of geometrical asperities on stress redistribution (Candela, Renard, Bouchon, *et al.*, 2011), coseismic slip distribution (Candela, Renard, Schmittbuhl, *et al.*, 2011) and propagation of the rupture during earthquakes (Klinger *et al.*, 2006; Vallée *et al.*, 2008).

Geodetic observations along several major continental faults have revealed, in addition to seismic slip during the coseismic phase, significant strain is released within the seismogenic portion of faults by aseismic slip, also known as creep, during the interseismic period (Burgmann *et al.*, 1998; Cavalié *et al.*, 2008; Jolivet *et al.*, 2012). Along strike-slip faults, the seismogenic zone can remain locked during the interseismic period or interseismic creep can occur from the surface to the transition zone at depth, affecting as a consequence the total budget of slip where it occurs (e.g., Ryder and Bürgmann, 2008; Jolivet *et al.*, 2012). An increasing number of observations reveals a wide variety of aseismic slip behaviors, from constant creep to episodic slow-slip events (e.g., Çakir *et al.*, 2003; Murray and Segall, 2005; Titus *et al.*, 2006; Chang *et al.*, 2009), often collocated with a variety of seismic events (e.g., Johanson and Burgmann, 2005; Shelly *et al.*, 2009), which raises the debate on the physical relationships between seismic and aseismic slip (Ide *et al.*, 2007; Peng and Gomberg, 2010). The behavior of creeping faults has often been interpreted in terms of effective frictional properties, with creeping sections corresponding to velocity-strengthening domains, whereas seismic faults would have velocity-weakening properties (Chang *et al.*, 2009; Barbot *et al.*, 2012). In the following, we will discuss a possible

*Now at COMET+, Bullard Labs, Department of Earth Sciences, University of Cambridge, Cambridge, United Kingdom.

†Also at Physics of Geological Processes, Department of Geosciences, University of Oslo, Norway.

physical interpretation of the slip behavior of faults, where the rough geometry of a fault produces a heterogeneous stress field and creates long-range elastic interactions that may control the rich dynamics of creep, as it has been proposed by Schmittbuhl *et al.* (2006).

A 30–40 km long creeping section has recently been identified using Interferometric Synthetic Aperture Radar (InSAR) along the Haiyuan fault, a major left-lateral fault at the northeastern boundary of the Tibetan plateau (Gaudemer *et al.*, 1995; Cavalié *et al.*, 2008; Jolivet *et al.*, 2012, 2013). Here, we focus on the dynamics of the observed shallow creep and on its relationship with fault geometry. This creeping section (from 37.11° N, 103.68° E to 37.00° N, 104.15° E) is located at the western end of the surface trace of the 1920 $\mathbf{M} \sim 8$ Haiyuan earthquake (Fig. 1) (Zhang *et al.*, 1987). It connects to the 1920 rupture trace through a major left stepover known to have influenced the propagation of large historical earthquakes (Liu-Zeng *et al.*, 2007). Geodetic investigations using InSAR suggest no significant slip deficit builds up along the creeping section on average over the 2003–2009 period, as it slips at plate loading rate (5 ± 1 mm/yr). Creep spatially coincides with a zone of micro- to moderate seismicity with a cumulative moment accounting for less than 3% of the total slip budget (Cavalié *et al.*, 2008; Jolivet *et al.*, 2012). Over the same period, this section experiences significant creep rate variations coeval to the largest earthquakes, suggesting the presence of local seismic asperities embedded in this creeping section, hence a certain roughness of the fault plane. However, the effective frictional properties of the fault zone derived from the average creep rate measured by InSAR over the whole creeping section suggest the observed fluctuations of aseismic slip rate in space and time are not driven by the observed seismicity (Jolivet *et al.*, 2013). Therefore, we propose to explore the role of the geometry of the fault on the dynamics of aseismic slip along this section.

Based on optical imagery and time series of InSAR data, we characterize the spatial correlations in the distribution of surface creep and in the fault geometry, comparing their roughness at all spatial scales. We then explore the temporal behavior of surface creep in the light of recent laboratory experiments, comparing it with generic characteristics of earthquakes.

InSAR Time-Series Analysis and Surface Creep along the Fault

To explore the spatial and temporal behavior of surface creep in greater detail, we use the InSAR time series derived by Jolivet *et al.* (2013) from radar data acquired by the Envisat satellite along ascending orbits on track 240. Data cover the 2003–2009 period, with monthly acquisitions since 2007. Other tracks analyzed in this previous study were discarded as they only partially cover the creeping section (tracks 469 and 333) or because of unconstrained temporal evolution of pixels in the fault zone due to disconnected subsets in the baseline/time domain (track 61) (see supplementary materials in Jolivet *et al.*, 2013). Below, we recall the main processing steps to obtain interferograms and invert for time series of ground displacement along the satellite line-of-sight.

We use ROI_PAC jointly with NSBAS to combine 25 Synthetic Aperture Radar (SAR) images into 74 interferograms (Rosen *et al.*, 2004; Doin *et al.*, 2011). From the raw SAR data, we build Single Look Complex images all coregistered to a single master image. Full resolution interferograms are computed using a range spectral filtering technique that adapts to local slope, to improve coherence in areas of rough topography (Guillaso *et al.*, 2006). Interferograms are then downsampled by a factor 4 in range and 20 in azimuth, filtered and unwrapped. Tropospheric phase delays and orbital ramps are empirically corrected and adjusted to ensure consistency between acquisitions, adapting the method from Cavalié *et al.* (2008). A detailed description of the processing of interferograms can be found in Jolivet *et al.* (2012).

Once all interferograms have been produced, we proceed to a time-series analysis of surface displacements around the creeping section of the Haiyuan fault using SAR acquisitions connected by at least two interferograms. We apply a generalized least-square approach and a temporal smoothing to remove uncorrelated atmospheric turbulent effects and solve for the phase value at each pixel and each acquisition date. A fully detailed description of the time-series processing can be found in Jolivet *et al.* (2013). In the following, we use the smoothed phase evolution, as it is devoid of high-frequency noise imposed by remaining atmospheric delays. As we focus on how strain is distributed in the near-fault zone, we subtract from the time series the long-wavelength deformation signal due to a 5 mm/yr long-term tectonic loading at depth (Jolivet *et al.*, 2012).

Along the 30–40 km long creeping section (Fig. 1), we explore the spatial and temporal fluctuations of surface creep at high-spatial resolution. Along the fault trace, every 45 m we use a 200 m wide, 8 km long profile perpendicular to the fault to measure the creep step across the fault trace and eventually derive the along-strike distribution of the surface creep for each time step of the data set, as done in Jolivet *et al.* (2013). We apply a median filter on each aseismic slip distribution to avoid short-wavelength noise due to phase scattering. Apparent dextral slip between two successive SAR acquisitions is considered as noise. Assuming no vertical motion and no fault perpendicular, horizontal slip, the resulting distributions of creep at each time step are finally projected onto the fault-parallel direction (Fig. 1).

Correlation and Self-Affinity of the Spatial Distribution of Shallow Creep and Fault Trace Geometry

A first striking feature is that the first-order segmentation, at the scale of about 10 km, of the along-strike distribution of creep is similar to that of the fault geometry of the Haiyuan fault. Two significant slip minima, separating three main sections, can be identified (at 10 and 25 km in Fig. 1)

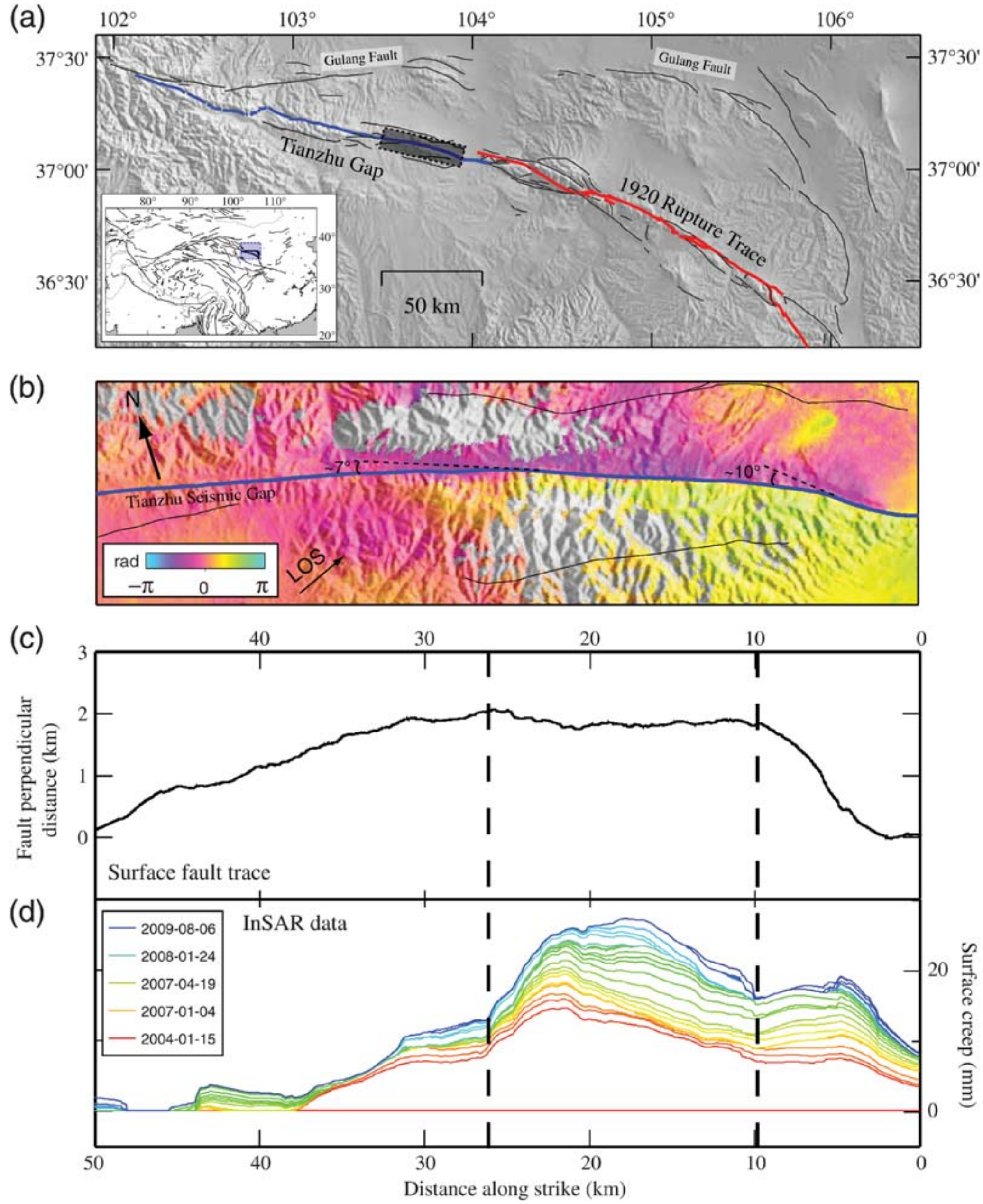

Figure 1. Fault geometry and aseismic slip distribution along the Haiyuan fault. (a) Map of the Haiyuan fault system, with the 1920 rupture trace (in red) and the millennial Tianzhu seismic gap (in blue). Dark lines indicate secondary faults. Gray shading is topography from Shuttle Radar Topography Mission (Farr and Kobrick, 2000). The inset indicates the localization of (a) in China. Gray shaded rectangle shows the area covered in (b). (b) Closeup map of the fault creeping section (blue line) and minor faults (dark lines). Gray shading indicates topography. Superimposed color pattern is the cumulative displacement along line of sight between 15 January 2004 and 06 August 2009 on ascending track 240. (c) Cartesian representation of the fault trace in a Universal Transverse Mercator projection. Vertical dashed lines indicate the two most significant fault bends. Black arrows indicate a possible second-order fault segmentation discussed in the text. (d) Cumulative aseismic distribution of fault-parallel slip measured along strike on ascending track 240 between 25 January 2004 and 06 August 2009. Colors indicate time of acquisitions.

and are collocated with the two most significant fault bends of ~10° and ~7°, respectively. A 2 km long, 500 m wide, extensional jog associated with the bend at km 25 is visible in the field, suggesting the long-lived configuration of this bend and the consistency of such geometrical segmentation at depth, at least for the first kilometers of the crust. At a smaller scale as well, the creep distribution shows variations that coincide with slight changes of fault strike. Such a correlation between local azimuth of the fault and average creep rate along strike over the 2003–2009 period has already been observed by Jolivet *et al.* (2013). In addition, segments of similar length are often identified along major

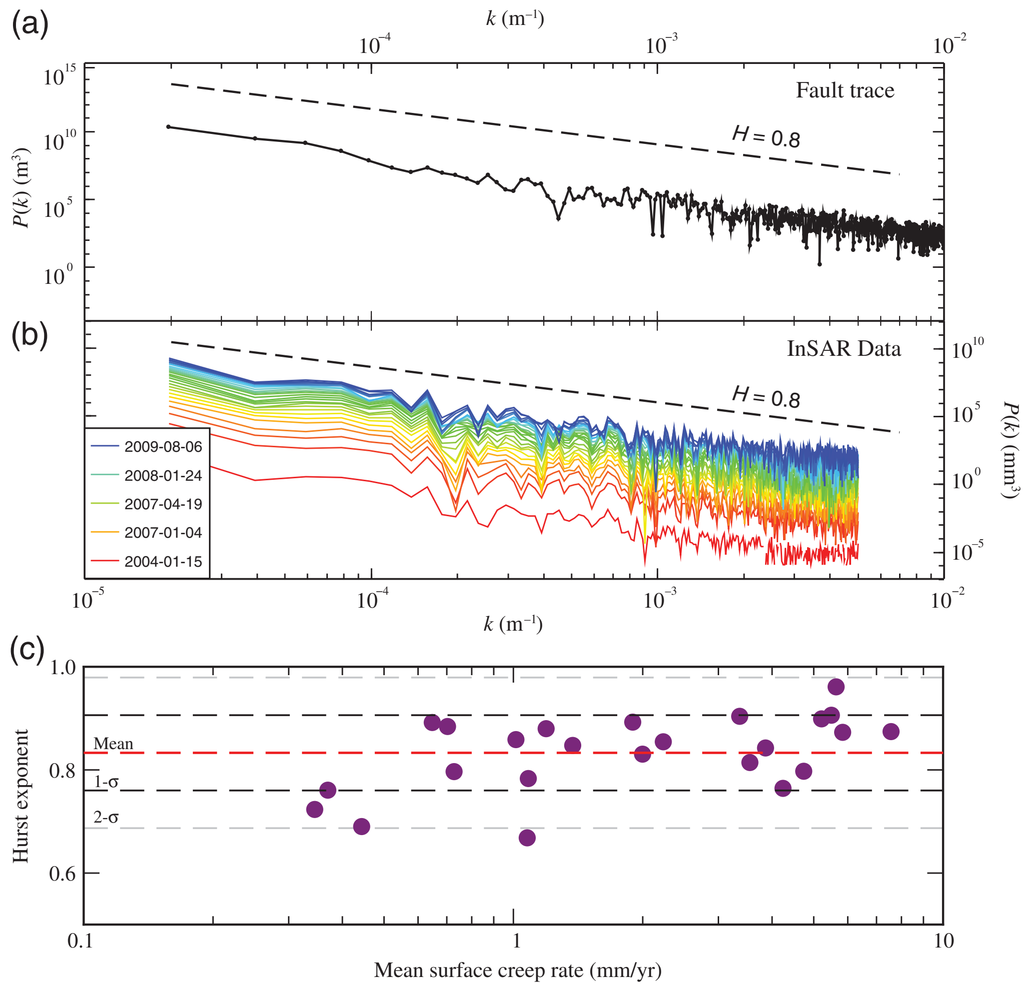

Figure 2. Roughness characterization. (a) Fourier power spectrum of the Haiyuan fault trace. Black dashed line is a power law with a Hurst exponent of 0.8. (b) Fourier power spectrum of fault-parallel aseismic slip distribution along the Haiyuan fault creeping section measured on track 240. Colors indicate time of acquisitions as in Figure 1. Curves have been shifted vertically for clarity. (c) Hurst exponent of slip distributions at each time step as a function of the average instantaneous creep rate measured between two successive time steps. Red dashed line is the mean Hurst exponent. Dark dashed lines indicate the 68% confidence interval (1-σ). Gray dashed lines indicate the 95% confidence interval (2-σ).

continental strike-slip faults in relationship with their seismic behavior (10–15 km long; e.g., Bilham and Williams, 1985; Klinger, 2010).

We further quantify the spatial correlations of aseismic slip and fault geometry at all scales. Following methodologies developed to study fault roughness (Power *et al.*, 1987; Candela, Renard, Bouchon, *et al.*, 2011; Candela, Renard, Schmittbuhl, *et al.*, 2011), we calculate the Fourier power spectrum $P(k)$ of the fault surface trace determined from field mapping and optical imagery (Gaudemer *et al.*, 1995; Lasserre *et al.*, 1999, 2002) (Fig. 2). The rough profile is first detrended by subtracting the line fit through the first and last points to avoid ramp artifacts in the Fourier analysis. We then derive the power spectrum (i.e., the square of the modulus of the Fourier transform) as a function of wavenumber k. The spectrum follows a power-law relationship, that is, a linear trend in a bilogarithmic plot (Fig. 2). We estimate the Hurst exponent H, defined as $P(k) \propto k^{-1-2H}$, with a linear least-squares regression on this linear trend.

The spectrum of the fault surface trace roughness can be approximated by a power law with a Hurst exponent $H = 0.8 \pm 0.1$, indicative of a self-affine regime. Under this particular regime, a few large-scale low-amplitude asperities are combined along the fault plane with a high number of small-scale large-amplitude asperities to produce roughness with no characteristic scale (Candela, Renard, Schmittbuhl, *et al.*, 2011). It is worth noting that a similar value of the Hurst exponent has been found for other major strike-slip continental faults, including the San Andreas fault and numerous faults of the eastern California shear zone (Candela, Renard, Schmittbuhl, *et al.*, 2011; Candela *et al.*, 2012). Such scaling relationship of fault roughness covers up to 11 orders of magnitude of length scales and has been interpreted as related to long-range elastic interactions during the quasistatic propagation of faults in the Earth's crust (Renard *et al.*, 2013). Models of fracture propagation have been proposed to explain the universality of the Hurst exponent (Hansen and Schmittbuhl, 2003).

We perform the same Fourier analysis of the spatial distribution of creep at each step of the time series (Fig. 2). All creep spatial distributions are characterized by a self-affine regime, as the spatial distribution of slip asperities follow a power law with a Hurst exponent $H = 0.8 \pm 0.1$, similar to the spatial distribution of geometrical asperities. This power-law behavior is independent of time, at least for a 6 year period, as no significant variation in Hurst exponents is measured from 2003 to 2009. In addition, we show that despite the observed significant temporal fluctuations of the surface creep rate (Fig. 3; Jolivet *et al.*, 2013), creep roughness is independent of mean creep velocity (Fig. 2).

Creep Bursts Dynamics

We now explore the size and velocity distributions of creep along the fault (Fig. 3). From the along-strike distribution of aseismic slip, we derive the along-strike distribution of the mean velocity between successive SAR acquisitions. We define a burst of creep as a segment where creep velocity is higher than a threshold value C at all points, an approach proposed to analyze laboratory data from analog experiments of slow propagating crack fronts (Måløy *et al.*, 2006). As the equivalent aseismic moment exceeds the measured seismic moment over the observation period (by a factor of 30, Jolivet *et al.*, 2012), we will assume these bursts are mostly aseismic. We vary C from 1 to 15 mm/yr and measure the along-strike length L and mean displacement $\bar{U}$ of each burst of creep.

To make a comparison with the seismic moment of earthquakes, defined as $M_0 = \mu DS$, in which μ is the shear modulus of the rock, D is the amount of slip during a given earthquake, and S is the slip surface area, we derive the potency of each burst of creep P as the product of slip and area, as follows:

$$P = \bar{U}L^2. \quad (1)$$

We assume the width of a creep burst is similar to its length to derive the area of slip, but more complex scalings between width and length of bursts would only shift the values toward lower potencies (if the scaling imposes cracks elongated in the along-strike direction, for instance). We use potency instead of seismic moment, because geodetic data are not sensitive to absolute shear modulus. Our analysis suggests the potency of bursts follows a power law with an exponent of approximately -1. This relationship between the number and the potency of creep bursts is analogous to the Gutenberg–Richter law, which describes the number of earthquakes as a function of their magnitude.

The potency of bursts being the combination of their length and slip, it is tempting to see which of these measurable quantities is responsible for this power-law behavior. The probability density function (PDF) of the length of bursts shows a clear power-law behavior, whereas the probability of slip is uniform from 0.1 to 1 mm (Fig. 4). Therefore, our sample set of bursts is made up of a similar quantity of small bursts with large slip, rather long bursts with low slip, hence the power-law behavior of the bursts potency derives from that of their length. This additional observation raises again geometrical considerations on the control of the burst activity.

We finally evaluate the distribution of creep rates (Fig. 3). This distribution is non-Gaussian, showing an asymmetrical PDF, with a skewness of about 1.9 (i.e., third moment of the distribution, Fig. 3) and a long tail toward large creep velocities. The maximum of the distribution is centered on 5 mm/yr, which corresponds to the present-day tectonic loading rate of the Haiyuan fault (Jolivet *et al.*, 2012). Possibly, faster bursts may have occurred during the observation period, but due to the temporal sampling of InSAR data, we are only able to access the average velocity between acquisitions. The distribution of creep velocities could exhibit an even longer tail toward fast creep events, as faster bursts could have been aliased by the uneven and loose sampling of the SAR acquisitions. The center of the distribution should likely remain equal to the long-term slip rate of the Haiyuan fault (i.e., around 5 mm/yr). Such value confirms low, or zero, strain accumulation during the period of observation across the creeping section (Jolivet *et al.*, 2012).

The presence of a long tail of large creep velocities has already been observed in several studies in material physics, focusing on the avalanche-like propagation of a front line into a heterogeneous media, such as mode I fractures (Måløy *et al.*, 2006; Tallakstad *et al.*, 2013) or imbibition fronts into a porous medium (Planet *et al.*, 2009). In these studies, non-Gaussian PDFs of velocity fluctuations, comparable to that in Figure 3c, have been related to the cascading of bursts and long-range interactions along the front. These distributions can be approximated using either generalized Gumbel distributions (Planet *et al.*, 2009) or stable Lévy distributions (Tallakstad *et al.*, 2013). Unfortunately, the noise in our data is too large to decipher between these two kinds of distributions. Nevertheless, the important result here is that fluctuations of creep velocity display a non-Gaussian distribution with an excess of fast bursts of creep.

Discussion: Origin of the Spatial Correlations

Our data suggest a spatial correlation at all scales between fault geometry and the distribution of aseismic slip at the surface. However, we do not know whether the spatial complexity of the creep distribution is confined to the surface only. Spatially coherent noise resulting from remaining turbulent atmospheric artifacts prevents us from estimating accurately the depth extent of creep bursts, whereas it reinforces our confidence in the precision of the measurement of surface creep (i.e., if the distance between two pixels is small, the corresponding phase difference is meaningful because these pixels covary, Jolivet *et al.*, 2013). However,

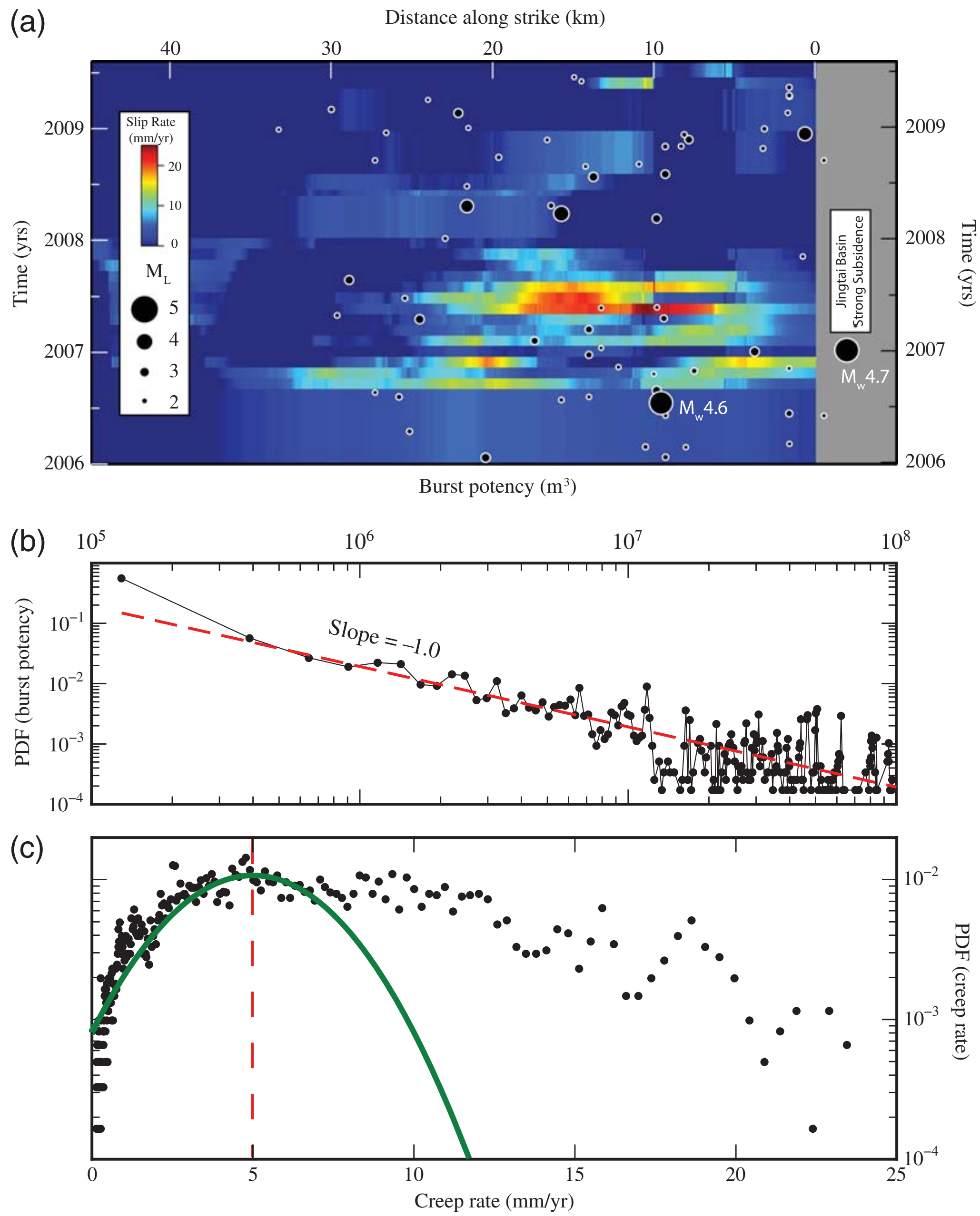

Figure 3. Characterizing the burst-like behavior. (a) Space and time distribution of the surface fault-parallel aseismic slip rate measured on track 240. The *x*-axis is along-strike distance, as in Figure 1. The *y*-axis is time. Colors show creep rate between two consecutive acquisitions. Creep rate is set to zero when measurements are negative. Gray area corresponds to a pull-apart basin, where strong subsidence is observed. Black dots indicate micro- and moderate seismicity. Uncertainty of the location is ±5 km. We extended the area to the east (gray area) where the largest earthquake is located. We do not find clear correlation between earthquakes and creep bursts, apart from the two largest events that resulted from an increase in creep rates along the whole segment (Jolivet *et al.*, 2013). (b) Empirical probability density function (PDF) of the burst potency as measured in (a) (dark dots). Dashed red line is a power law with a −1.0 exponent. (c) Empirical PDF of the aseismic slip velocity (dark dots). Measured skewness of the distribution is 1.9. Green line is the Gaussian distribution. The distribution is centered on 5 mm/yr, with a 2.2 mm/yr standard deviation.

aseismic slip is homogeneously distributed between the surface and 20 km depth on average over the 2003–2009 period (Jolivet *et al.*, 2012). In addition, because fault perpendicular profiles of the ground displacement resemble step functions, creep is definitely not confined to the few tenths of meters near the surface but rather spans the first kilometers at depth (Jolivet *et al.*, 2013). We, therefore, consider the along-strike distributions of aseismic slip, which we measure, most likely result from deformation mechanisms spanning at least the first few kilometers of the crust at depth.

The power-law exponents of fault and slip roughness have a similar value. We acknowledge correlation does not

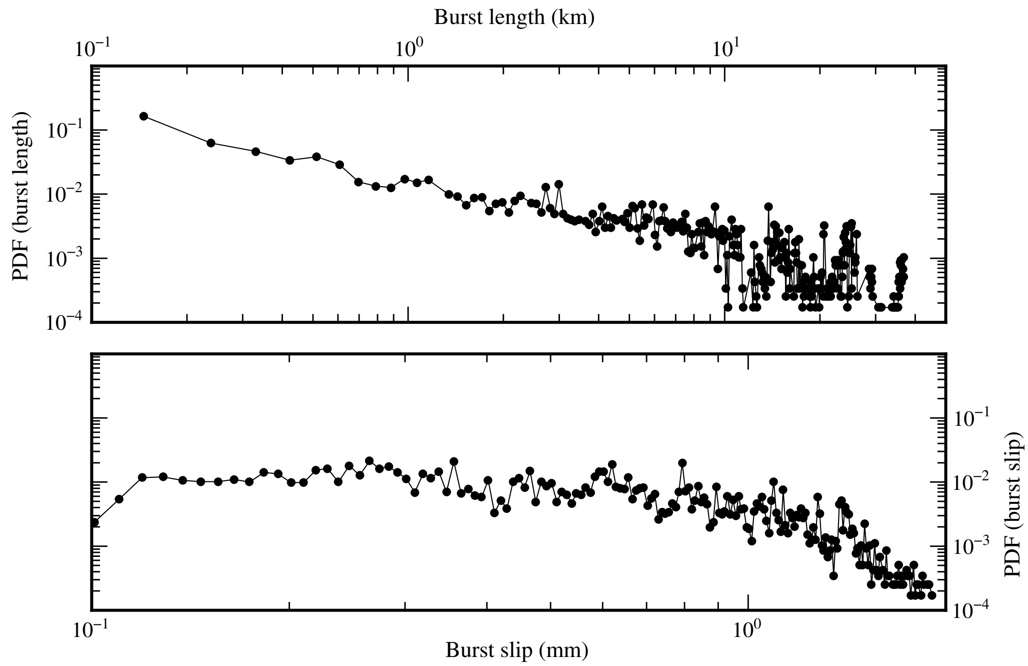

Figure 4. Probability of bursts length and slip. (a) PDF of the length of the bursts of creep identified in Figure 3. The PDF shows a power-law behavior from which derives the power-law behavior of the potency of bursts. (b) PDF of the slip of bursts. The probability is uniform between 0.1 and 1 mm of slip, showing that our sample set is homogeneously distributed between these values.

demand causality, but our observations are consistent with a geometrical control of creep during the period of observation along this section of the fault. Analog experiments of crack propagation on an interface with controlled roughness exhibit similar behavior (Schmittbuhl and Måløy, 1997). A similar mechanism could be involved with the occurrence of repeating earthquakes, in which the same asperity exerts a control on local stress and breaks at regular time intervals. Here, our interpretation is that the geometry of the fault exerts a similar control on creep.

As the power law describing the distribution of creep does not change with time (Fig. 2), we suggest that no temporal smoothing of the fault surface happens during the period of observation. Still, constantly reorganizing asperities could explain such observation (Candela, Renard, Bouchon, *et al.*, 2011). However, as the shape of the slip distribution is also stable through time (Fig. 2), we favor a simpler explanation in which geometrical asperities, which concentrate strain and release it aseismically, are persistent over the study period. Again, such behavior echoes the repeating earthquakes observed at Parkfield, California (Nadeau and McEvilly, 1999), and the microearthquake lineaments observed along the Hayward fault, California (Rubin *et al.*, 1999), where (in both cases) no apparent alteration of asperities through time is documented during the interseismic period. Although this situation is stable over the observation period, it is not consistent on the long run, and the slip pattern needs to adapt in the future to release local strain deficit, either through seismic or aseismic slip.

Bursts of creep have already been observed in experimental analogs. Laboratory experiments have shown the quasi-static propagation of a slow rupture front along a plane with controlled roughness results from the successive ruptures of geometrical asperities (Måløy *et al.*, 2006; Lengliné *et al.*, 2012; Tallakstad *et al.*, 2013). Also, similar experiments have shown that the self-affinity of a slow fracture front propagating along a plane does not depend on the crack velocity but is controlled by the bulk properties of the surrounding heterogeneous medium (Schmittbuhl and Måløy, 1997). In all these experiments, the key ingredient that explains the observed power-law relationships is the presence of long-range interactions into a disordered medium. Such interactions may lead to non-Gaussian distributions of creep velocity, as observed for the Haiyuan fault. Making the analogy between our observations with such experiments and numerical models (Candela, Renard, Schmittbuhl, *et al.*, 2011), we propose that the elasticity of the brittle crust imposes long-distance interactions between geometrical asperities (Schmittbuhl and Måløy, 1997), that in turn control the spatial distribution of the creep.

We interpret the observed dynamics of creep as resulting from the competition between elastic deformation processes driven by the tectonic loading and controlled by the elasticity of the surrounding crust, and the cascading of creep bursts. Our interpretation is that, if creep bursts were not cascading, the distribution of aseismic slip velocities should be symmetric, centered on the average creep rate for the whole segment. In other words, the observed aseismic slip results from the addition of aseismic slip events of all scales, referred to as bursts of creep, that are interacting with each other, while being spatially constrained by the distribution of geometrical asperities along the Haiyuan fault.

Conclusion

We derive the temporal evolution of along-strike distributions of aseismic slip along the surface trace of the Haiyuan fault creeping section. We observe spatial correlations, at all spatial scales and persistent at least during the observation period, of the distribution of aseismic asperities, referred to as bursts of creep. A correlation at all scales with the surface trace of the fault is also characterized. We then evaluate the dynamics of creep bursts. Our objective is to improve our understanding of aseismic slip behavior by exploring a possible control of slip by fault geometry.

First, we emphasize the fact that all our observations are similar to those made on laboratory experiments modeling the propagation of a slow rupture front on a rough interface. Second, we note the behavior of creep bursts resembles the time behavior of earthquakes. The spatial and temporal distribution of aseismic slip as well as the potency of creep bursts may be explained by mechanisms similar to the brittle behavior of the seismogenic upper crust: (1) the potency of creep bursts follows a power law, similar to the Gutenberg–Richter law, and (2) creep bursts interact with each other, resulting in a strongly asymmetric distribution of creep velocities. Consequently, we consider that our observations do favor the existence of a continuum between earthquakes and aseismic slip along active faults (Peng and Gomberg, 2010) and that long-range elastic interactions into a heterogeneous Earth's crust may control the rich dynamics observed for both dynamic ruptures and creep events.

Data and Resources

Envisat images were provided by the Dragon program (ID 2509 and 5305) in collaboration between the European Space Agency and the National Remote Sensing Center of China.

Acknowledgments

The Dragon program (ID 2509 and 5305) supported R. Jolivet's work, through the Young Scientist fellowship. Funding was provided by the Agence Nationale de la Recheche (ANR) Extraction et Fusion d'Information et de Données d'Interférométrie Radar (EFIDIR) and Programme National de Télédétection Spatiale (Centre National d'Etudes Spatiales [CNES]), and ANR-JCJC-0011-01 grant. This study was funded by the Labex OSUG@2020 (Investissement dAvenir ANR10-LABX56). We thank Knut Jørgen Måløy for helpful discussions on the long-tail distributions of velocity fluctuations.

References

Adda-Bedia, M., and R. Madariaga (2008). Seismic radiation from a kink on an antiplane fault, *Bull. Seismol. Soc. Am.* **98,** no. 5, 2291–2302, doi: 10.1785/0120080003.

Barbot, S., N. Lapusta, and J. P. Avouac (2012). Under the hood of the earthquake machine: Toward predictive modeling of the seismic cycle, *Science* **336,** no. 6082, 707–710, doi: 10.1126/science.1218796.

Bilham, R., and P. Williams (1985). Sawtooth segmentation and deformation processes on the southern San Andreas fault, California, *Geophys. Res. Lett.* **12,** no. 9, 557–560.

Burgmann, R., E. Fielding, and J. Sukhatme (1998). Slip along the Hayward fault, California, estimated from space-based synthetic aperture radar interferometry, *Geology* **26,** no. 6, 559–562.

Çakir, Z., J.-B. de Chabalier, R. Armijo, B. Meyer, A. Barka, and G. Peltzer (2003). Coseismic and early post-seismic slip associated with the 1999 Izmit earthquake (Turkey), from SAR interferometry and tectonic field observations, *Geophys. J. Int.* **155,** no. 1, 93–110, doi: 10.1046/j.1365-246X.2003.02001.x.

Candela, T., F. Renard, M. Bouchon, J. Schmittbuhl, and E. E. Brodsky (2011). Stress drop during earthquakes: Effect of fault roughness scaling, *Bull. Seismol. Soc. Am.* **101,** no. 5, 2369–2387, doi: 10.1785/0120100298.

Candela, T., F. Renard, Y. Klinger, K. Mair, J. Schmittbuhl, and E. E. Brodsky (2012). Roughness of fault surfaces over nine decades of length scales, *J. Geophys. Res.* **117,** B08409, doi: 10.1029/2011JB009041.

Candela, T., F. Renard, J. Schmittbuhl, M. Bouchon, and E. E. Brodsky (2011). Fault slip distribution and fault roughness, *Geophys. J. Int.* **197,** no. 2, 957–968, doi: 10.1111/j.1365-246X.2011.05189.x.

Cavalié, O., C. Lasserre, M. P. Doin, G. Peltzer, J. Sun, X. Xu, and Z. K. Shen (2008). Measurement of interseismic strain across the Haiyuan fault (Gansu, China), by InSAR, *Earth Planet. Sci. Lett.* **275,** nos. 3/4, 246–257, doi: 10.1016/j.epsl.2008.07.057.

Chang, S.-H., W.-H. Wang, and J.-C. Lee (2009). Modelling temporal variation of surface creep on the Chihshang fault in eastern Taiwan with velocity-strengthening friction, *Geophys. J. Int.* **176,** no. 2, 601–613, doi: 10.1111/j.1365-246X.2008.03995.x.

Doin, M. P., S. Guillaso, R. Jolivet, C. Lasserre, F. Lodge, G. Ducret, and R. Grandin (2011). Presentation of the small baseline NSBAS processing chain on a case example: The Etna deformation monitoring from 2003 to 2010 using ENVISAT data, in *Proceedings of the Fringe Symposium*, Frascati, Italy, 19–23 September 2011, Eur. Space Agency Spec. Publ.

Farr, T. G., and M. Kobrick (2000). Shuttle radar topography mission produces a wealth of data, *Eos Trans. AGU* **81,** no. 48, 583–585.

Gaudemer, Y., P. Tapponnier, B. Meyer, G. Peltzer, S. M. Guo, Z. T. Chen, H. G. Dai, and I. Cifuentes (1995). Partitioning of crustal slip between linked, active faults in the eastern Qilian Shan, and evidence for a major seismic gap, the Tianzhu gap, on the western Haiyuan fault, Gansu (China), *Geophys. J. Int.* **120,** no. 3, 599–645.

Guillaso, S., A. Reigber, L. Ferro-Famil, and E. Pottier (2006). Range resolution improvement of airborne SAR images, *IEEE Trans. Geosci. Remote Sens.* **3,** no. 1, 135–139, doi: 10.1109/LGRS.2005.859943.

Hansen, A., and J. Schmittbuhl (2003). Origin of the universal roughness exponent of brittle fracture surfaces: Stress-weighted percolation in the damage zone, *Phys. Rev. Lett.* **90,** no. 4, doi: 10.1103/PhysRevLett.90.045504.

Ide, I., G. C. Beroza, D. R. Shelly, and T. Uchide (2007). A scaling law for slow earthquakes, *Nature* **447,** 76–79, doi: 10.1038/nature05780.

Johanson, I., and R. Burgmann (2005). Creep and quakes on the northern transition zone of the San Andreas fault from GPS and InSAR data, *Geophys. Res. Lett.* **32,** no. 14, doi: 10.1029/2005GL023150.

Jolivet, R., C. Lasserre, M. P. Doin, S. Guillaso, G. Peltzer, R. Dailu, J. Sun, Z. K. Shen, and X. Xu (2012). Shallow creep on the Haiyuan fault (Gansu, China) revealed by SAR interferometry, *J. Geophys. Res.* **117,** no. B6, doi: 10.1029/2011JB008732.

Jolivet, R., C. Lasserre, M. P. Doin, G. Peltzer, J.-P. Avouac, R. Dailu, and J. Sun (2013). Spatio-temporal evolution of aseismic slip along the Haiyuan fault, China: Implications for fault frictional properties, *Earth Planet. Sci. Lett.* **377/378,** 23–33, doi: 10.1016/j.epsl.2013.07.020.

King, G., and J. Nabelek (1985). Role of fault bends in the initiation and termination of earthquake rupture, *Science* **228,** no. 4702, 984–987, doi: 10.1126/science.228.4702.984.

Klinger, Y. (2010). Relation between continental strike-slip earthquake segmentation and thickness of the crust, *J. Geophys. Res.* **115,** no. B07306, doi: 10.1029/2009JB006550.

Klinger, Y., R. Michel, and G. C. P. King (2006). Evidence for an earthquake barrier model from $M_w \sim 7.8$ Kokoxili (Tibet) earthquake slip-distribution, *Earth Planet. Sci. Lett.* **242,** 354–364, doi: 10.1016/j.epsl.2005.12.003.

Lasserre, C., Y. Gaudemer, P. Tapponnier, A. S. Meriaux, J. Van der Woerd, D. Y. Yuan, F. J. Ryerson, R. C. Finkel, and M. W. Caffee (2002). Fast late Pleistocene slip rate on the Leng Long Ling segment of the Haiyuan fault, Qinghai, China, *J. Geophys. Res.* **107,** no. B11, 2276, doi: 10.1029/2000JB000060.

Lasserre, C., P.-H. Morel, Y. Gaudemer, P. Tapponnier, F. J. Ryerson, G. C. P. King, F. Metivier, M. Kasser, M. Kashgarian, L. Baichi, L. Taiya, and Y. Daoyang (1999). Postglacial left slip rate and past occurrence of M 8 earthquakes on the western Haiyuan fault, Gansu, China, *J. Geophys. Res.* **104,** no. B8, 17,633–17,651, doi: 10.1029/1998JB900082.

Lasserre, C., G. Peltzer, F. Crampé, Y. Klinger, J. Van der Woerd, and P. Tapponnier (2005). Coseismic deformation of the 2001 $M_w = 7.8$ Kokoxili earthquake in Tibet, measured by synthetic aperture radar interferometry, *J. Geophys. Res.* **110,** no. B12, doi: 10.1029/2004JB003500.

Lengliné, O., J. E. Elkhoury, G. Daniel, J. Schmittbuhl, R. Toussaint, J. P. Ampuero, and M. Bouchon (2012). Interplay of seismic and aseismic deformations during earthquake swarms: An experimental approach, *Earth Planet. Sci. Lett.* **331/332,** 215–223, doi: 10.1016/j.epsl.2012.03.022.

Liu-Zeng, J., Y. Klinger, X. Xu, C. Lasserre, G. Chen, W. Chen, P. Tapponnier, and B. Zhang (2007). Millennial recurrence of large earthquakes on the Haiyuan fault near Songshan, Gansu Province, China, *Bull. Seismol. Soc. Am.* **97,** no. 1B, 14–34, doi: 10.1785/0120050118.

Måløy, K. J., S. Santucci, J. Schmittbuhl, and R. Toussaint (2006). Local waiting time fluctuations along a randomly pinned crack front, *Phys. Rev. Lett.* **96,** no. 4, doi: 10.1103/PhysRevLett.96.045501.

Murray, J. R., and P. Segall (2005). Spatiotemporal evolution of a transient slip event on the San Andreas fault near Parkfield, California, *J. Geophys. Res.* **110,** no. B09407, doi: 10.1029/2005JB003651.

Nadeau, R. M., and T. V. McEvilly (1999). Fault slip rates at depth from recurrence intervals of repeating microearthquakes, *Science* **285,** 718.

Peng, Z., and J. Gomberg (2010). An integrated perspective of the continuum between earthquakes and slow-slip phenomena, *Nat. Geosci.* **3,** no. 9, 599–607, doi: 10.1038/ngeo940.

Planet, R., S. Santucci, and J. Ortin (2009). Avalanches and non-Gaussian fluctuations of the global velocity of imbibition fronts, *Phys. Rev. Lett.* **102,** no. 9, doi: 10.1103/PhysRevLett.102.094502.

Power, W. L., T. E. Tullis, S. R. Brown, G. N. Boitnott, and C. H. Scholz (1987). Roughness of natural fault surfaces, *Geophys. Res. Lett.* **14,** no. 1, 29–32, doi: 10.1029/GL014i001p00029.

Renard, F., T. Candela, and E. Bouchaud (2013). Constant dimensionality of fault roughness from the scale of micro-fractures to the scale of continents, *Geophys. Res. Lett.* **40,** no. 1, 83–87, doi: 10.1029/2012GL054143.

Rosen, P., S. Hensley, G. Peltzer, and M. Simons (2004). Updated repeat orbit interferometry package released, *Eos Trans. AGU* **85,** no. 5, 47.

Rubin, A., D. Gillard, and J. Got (1999). Streaks of microearthquakes along creeping faults, *Nature* **400,** no. 6745, 635–641.

Ryder, I., and R. Bürgmann (2008). Spatial variations in slip deficit on the central San Andreas fault from InSAR, *Geophys. J. Int.* **175,** no. 3, 837–852.

Schmittbuhl, J., and K. Måløy (1997). Direct observation of a self-affine crack propagation, *Phys. Rev. Lett.* **78,** no. 20, 3888–3891, doi: 10.1103/PhysRevLett.78.3888.

Schmittbuhl, J., G. Chambon, A. Hansen, and M. Bouchon (2006). Are stress distributions along faults the signature of asperity squeeze? *Geophys. Res. Lett.* **33,** L13307, doi: 10.1029/2006GL025952.

Shelly, D. R., W. L. Ellsworth, T. Ryberg, C. Haberland, G. S. Fuis, J. Murphy, and R. Bürgmann (2009). Precise location of San Andreas fault tremors near Cholame, California using seismometer clusters: Slip on the deep extension of the fault? *Geophys. Res. Lett.* **36,** L01303, doi: 10.1029/2008GL036367.

Tallakstad, K. T., R. Toussaint, S. Santucci, and K. J. Måløy (2013). Non-gaussian nature of fracture and the survival of fat-tail exponents, *Phys. Rev. Lett.* **110,** no. 14, 145501.

Titus, S. J., C. DeMets, and B. Tikoff (2006). Thirty-five-year creep rate for the creeping segment of the San Andreas fault and the effects of the 2004 Parkfield earthquake: Contraints from alignment arrays, continuous Global Positioning System, and creepmeters, *Bull. Seismol. Soc. Am.* **96,** no. 4B, S250–S268, doi: 10.1785/0120050811.

Vallée, M., M. Landès, N. M. Shapiro, and Y. Klinger (2008). The 14 November 2001 Kokoxili (Tibet) earthquake: High-frequency seismic radiation originating from the transition between sub-Rayleigh and supershear rupture velocity regimes, *J. Geophys. Res.* **113,** no. B07305, doi: 10.1029/2007JB005520.

Wesnousky, S. G. (2006). Predicting the endpoints of earthquake ruptures, *Nature* **444,** no. 7117, 358–360, doi: 10.1038/nature05275.

Zhang, W. Q., D. C. Jiao, P. Z. Zhang, P. Molnar, B. C. Burchfield, Q. D. Deng, Y. P. Wang, and F. M. Song (1987). Displacement along the Haiyuan fault associated with the great 1920 Haiyuan, China, earthquake, *Bull. Seismol. Soc. Am.* **77,** no. 1, 117–131.

Seismological Laboratory
Department of Geological and Planetary Sciences
California Institute of Technology
1200 E California Boulevard
Pasadena, California 91125
jolivetinsar@gmail.com
(R.J.)

Department of Geosciences
Pennsylvania State University
542 Deike Building
University Park, Pennsylvania 16801
(T.C.)

ISTerre, Université Grenoble Alpes
CNRS, BP 53
38041 Grenoble, France
(C.L., F.R., M.-P.D.)

Institut de Physique du Globe
Sorbonne Paris cité
Univ. Paris Diderot
CNRS UMR 7154
75005 Paris, France
(Y.K.)

Manuscript received 6 August 2014;
Published Online 30 December 2014